31 August 2001

ELSEVIER

Chemical Physics Letters 344 (2001) 479–487

CHEMICAL PHYSICS LETTERS

www.elsevier.com/locate/cplett

Electronic spectrum of atomic sulfur in argon matrices in the vacuum ultraviolet region

Murthy S. Gudipati *, Andreas Klein

Institut für Physikalische Chemie, Universität zu Köln, Luxemburger Strasse 116, D-50939 Köln, Germany

Received 8 May 2001; in final form 28 June 2001

Abstract

S atoms have been generated through vacuum ultraviolet photolysis of carbonyl sulfide (OCS) in Ar matrices. Excitation spectra measured by monitoring the $^1S \rightarrow {}^1D$ emission of S at 784 nm are assigned to $Ar^+S^- \leftarrow ArS$ charge-transfer (CT) (135 nm, substitutional site (SS) and 159 nm, interstitial site (IS)) and $^3S \leftarrow {}^3P$ Rydberg (160.8 nm) transitions. Empirically derived potential curves of Rg^+S^- and Rg^+O^- species predict the transition energies with reasonable accuracy. S atoms are found to be more photomobile than O atoms in Ar matrices.

1. Introduction

The recently emerging emphasis of matrix isolation as a means to study and understand many body interactions in condensed media [1] has furthered the conventional matrix isolation, a means to stabilize otherwise unstable species in low-temperature inert media, to utilize rare gases themselves as reactive media. Thus *inert gas* as synonym to *rare gas* has been shown to be invalid at least in the case of Ar, Kr and Xe. With dopant atoms like hydrogen, halogen, oxygen, sulfur etc., rare gases form locally generated stable or metastable ground-state molecules [2,3] or excited species [1,4]. Due to the presence of several equivalent rare gas atoms surrounding the dopant atoms, it still remains a challenging theoretical problem to describe the nature and composition of the excited species, especially of charge-transfer (CT) nature.

In our earlier Letter on O doped Ar and Kr matrices [4], we could understand to a large extent the CT and Rydberg transitions of O in rare gas matrices. We have shown that the empirical potential energy curves of the CT states, after taking into account the stabilization through host matrix polarizability, could be used to predict the excitation energies with a reasonable accuracy. To the best of our knowledge, so far there has been no literature data on the absorption or emission spectra involving ArS or KrS CT states either in the gas-phase or in rare gas matrices. On the other hand, emission spectra of XeS involving the CT states have been measured both in the gas-phase [5] and in Xe matrices [6]. Ab initio potential energy curves of KrS [7] and XeS [8] CT states have been reported, but not of ArS. In the present communication we report the first observation of ArS CT transitions and the $S(^3S \leftarrow {}^3P)$ atomic

* Corresponding author. Fax: +49-221-470-5144.

E-mail address: murthy.gudipati@uni-koeln.de (M.S. Gudipati).

0009-2614/01/$ - see front matter
PII: S0009-2614(01)00803-X

transition in a rare-gas matrix. The experimental results are compared with empirical predictions. The present work may be a useful reference point to both theoretical and experimental investigations on RgS in the future.

2. Experimental

The experiments have been carried out at the synchrotron radiation facility BESSY-I in Berlin using a 3 m normal incidence (3m-NIM-1) monochromator. Emission spectra were measured using a 0.5 m monochromator (Acton Research, SpectraPro-500). Transmission spectra were simultaneously measured with an InGaAs photodiode (Hamamatsu) when recording the excitation spectra. Due to the fact that the horizontal and vertical foci of the 3m-NIM-1 monochromator do not spatially coincide with each other, the irradiated spot on the matrix window (FWHM) was approximately $4(\mathrm{H}) \times 2(\mathrm{V})$ mm^2, consisting of a central high-flux region and a peripheral low-flux region. While measuring the transmission spectra, all the transmitted light has been detected on the 5×5 mm^2 photodiode. In order to measure the emission and excitation spectra, the spot on the matrix window was imaged on to the entrance slits (opened to 1 mm) of the emission monochromator. Hence, only the central 1 mm (H) stripe of the irradiated matrix receiving the maximum amount of photon flux was interrogated through the emission and excitation spectra, whereas the transmission measurements covered a wider area on the matrix. Thus, subtle changes in the excitation spectra may not be detected in the transmission spectra and a quantitative comparison between the excitation and transmission spectra cannot be carried out. All the experimental details are given in earlier publications [4,9]. Sulfur atoms were produced through photolysis of 0.1% OCS in Ar matrices while measuring excitation and emission spectra at excitation wavelengths between 200 and 100 nm. A premixed 5.76% OCS in Ar was further diluted with Ar (both from Linde) to achieve the desired concentration. The spectra were recorded at the lowest temperature (21 K) reachable with our cryostat.

3. Results and discussion

3.1. Spectral analysis

Excitation spectra measured while monitoring the $^1\mathrm{S} \rightarrow {}^1\mathrm{D}$ emission of S at 784 nm from a freshly prepared and during the photolysis of 0.1% OCS in an Ar matrix are shown in Fig. 1. The dissociative excitation of OCS to produce S(^{1}S) and CO($^1\Sigma^+$) is well studied in the gas-phase [10]. In Ar matrices Taylor et al. [11] have reported a similar spectrum with an irregularly spaced vibrational progression. The longer wavelength part between 145 and 175 nm consists of transitions into two upper valence states as shown in Fig. 1. The unresolved shoulder due to the $^1\Pi \leftarrow \mathrm{X}^1\Sigma^+$ transition at 165 nm is a clearly resolved broad band in the gas-phase absorption spectrum with the maximum at 167 nm [12]. The absorption maximum of the $^1\Sigma^+ \leftarrow \mathrm{X}^1\Sigma^+$ transition at 152 nm is in good agreement with the well-resolved regular vibronic structure with a vibrational spacing of $\sim$800 cm^{-1} centered at 152 nm [12]. The sharp band at 145 nm is characteristic of transition into the upper state of Rydberg character. Keeping in mind the general tendency of Rydberg states being shifted to higher energies in rare-gas matrices [13], we assign this band at 145 nm to the $^1\Pi(R) \leftarrow \mathrm{X}^1\Sigma^+$ ($3\pi \rightarrow \mathrm{ns}\sigma$ series, $3\pi \rightarrow 11\sigma$)

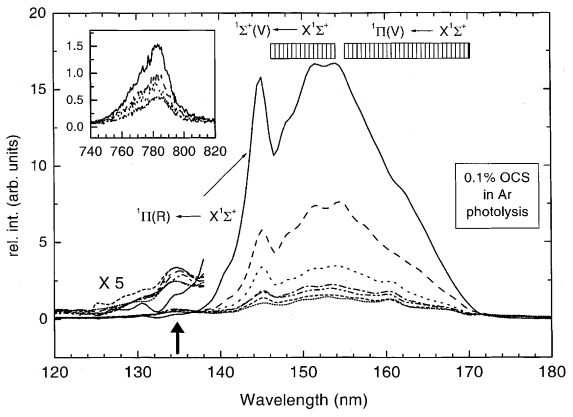

Fig. 1. Excitation spectra of OCS in Ar matrices with increasing photolysis (monitoring the $^1\mathrm{S} \rightarrow {}^1\mathrm{D}$ emission of S at 784 nm). Dispersed $^1\mathrm{S} \rightarrow {}^1\mathrm{D}$ emission of S during the photolysis is shown in the insert (excitation at 149 nm).

transition observed at 158 nm in the gas-phase [12]. All the other Rydberg transitions occur at shorter wavelengths than 145 nm in the gas-phase. As can be seen in Fig. 1, OCS is efficiently photolyzed up to >90% during the measurements with monochromatic synchrotron light in the region between 200 and 100 nm. The spectral intensity decreases more or less uniformly upon photolysis throughout, except for the region between 130 and 140 nm, enlarged and marked with an arrow in Fig. 1. In this region where the absorption of OCS is almost negligible, instead of decreasing, the spectral intensity increases slightly upon photolysis, which can be attributed to the S atoms that are formed during the photolysis.

We have also followed the generation of the photoproducts in the transmission spectra. These spectra, displaced vertically to gain clarity, are summarized in Fig. 2. It should be noted that light scattering is even more a serious problem in the vaccum ultraviolet (VUV) region compared to the UV and visible region. Thus, it is very difficult to differentiate between scattering and absorption when the transitions involve broad and weak absorption. Further, the optical quality of the matrices with respect to the VUV light change significantly upon photolysis. Keeping these aspects in mind, we did not over interpret the broad continua. Excitation spectroscopy is much more sensitive than the absorption spectroscopy to measure weak and broad bands in the VUV region (vide infra). In the transmission spectra shown in Fig. 2a, one can clearly notice an increase in the several absorption bands below 157 nm due to CO and the band at 160.8 nm due to the $^3S(3s^23p^34s) \leftarrow {}^3P(3s^23p^4)$ atomic transition of S with increasing photolysis, indicating the generation of CO and S photoproducts upon photodissociation of OCS.

These transmission spectra were converted to absorption spectra by taking the first transmission spectrum during the photolysis as the reference spectrum. These spectra after removing the continua are shown in Fig. 2b. If we assume that the oscillator strengths measured in the gas-phase for the corresponding transitions to hold good also in the matrix environment, then the integrated intensity of the $^3S \leftarrow {}^3P$ transition of S ($f = 0.093$ [14]) should be 5.74 times stronger than the A–X(0-0) band of CO ($f = 0.0162$ [15]) at 156.3 nm and 2.65 times stronger than the A–X(1-0) band of CO($f = 0.0351$ [15]) at 152.8 nm. The respective integrated intensity ratios, being 4.3 and 2.2 at the initial stages of the photolysis, decrease with increasing photolysis to final values of 1.8 and 1.1, respectively. When the matrices were

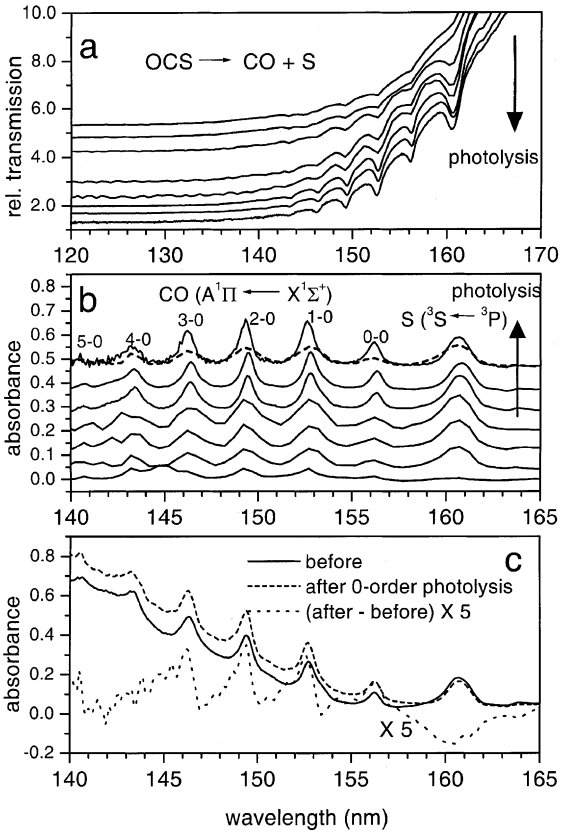

Fig. 2. (a) Transmission spectra measured during the photolysis of OCS, displaced vertically to enhance the clarity. The Ar matrices with 0.1% OCS are virtually non-transparent below 135 nm. (b) Spectra from part a converted to absorbance units, by taking the first measured transmission spectrum as the reference spectrum. The spectra were corrected to the background continuum. Second spectrum from the bottom has been shown again under the top spectrum as dashed curve to compare the relative intensities of the bands of CO and S that are produced with increasing photolysis of OCS. (c) Absorption spectra measured after 90% photolysis of OCS. Before (solid line) and after (dashed line) irradiation with undispersed synchrotron light. The difference spectrum (after – before) enlarged five times is also shown (dotted line).

irradiated with undispersed synchrotron light after about 90% photolysis of OCS, the absorption bands of CO increase whereas the absorption band due to S decreases, as shown in Fig. 2c. Hence, we conclude that VUV photolysis of OCS renders CO and S species in Ar matrices and S atoms are simultaneously photomobilized to undergo recombination to form S_2 or react with O atoms to form SO under the present experimental conditions. Prolonged photolysis thus depletes almost 50% of S atoms generated through photodissociation of OCS. Further evidence for the photoinduced mobility of the S atoms will be presented below.

In Fig. 3a excitation spectra during the photolysis and at the end of the photolysis and a difference spectrum after rescaling the 145 nm bands in both the spectra are shown. The difference spectrum, enlarged and fitted with two Gaussian curves is shown in Fig. 3b. These spectra are reminiscent of the spectra of O atoms in Ar matrices obtained through photolysis of N_2O precursor [16], where the precursor spectrum strongly overlapping with the product spectrum. We may note that these excitation spectra were measured by monitoring the ^1S–^1D-emission of S. Population of S(^1S) can only be achieved either through photodissociation of the OCS precursor or excitation of S in Ar lattice. The other minor photoproducts CS and SO cannot be dissociated in this spectral region to generate S(^1S). Hence, the difference spectrum must belong to S in Ar matrix. Further, the excitation spectra of CS and SO differ significantly from the spectrum shown in Fig. 3b (to be published elsewhere). Several interesting features can be detected in the subtracted spectrum. The sharp band at 160.8 nm is clearly the dominant feature that is due to the $^3S(3s^23p^34s) \leftarrow {}^3P(3s^23p^4)$ atomic transition in S. As noted earlier, matrix destabilization of the Rydberg states of small molecules in rare-gas matrices is a well-known fact [13]. In the gas-phase this $^3S \leftarrow {}^3P$ transition occurs at 180.7 nm [17]. The blue-shift of around 20 nm, corresponding to 0.84 eV for S in Ar matrices is larger than the blue-shift of 0.69 eV for the same transition in O in Ar matrices [4]. Greater destabilization of the ^3S Rydberg state of S compared to the same state of O in Ar matrices is due to the fact that in the case

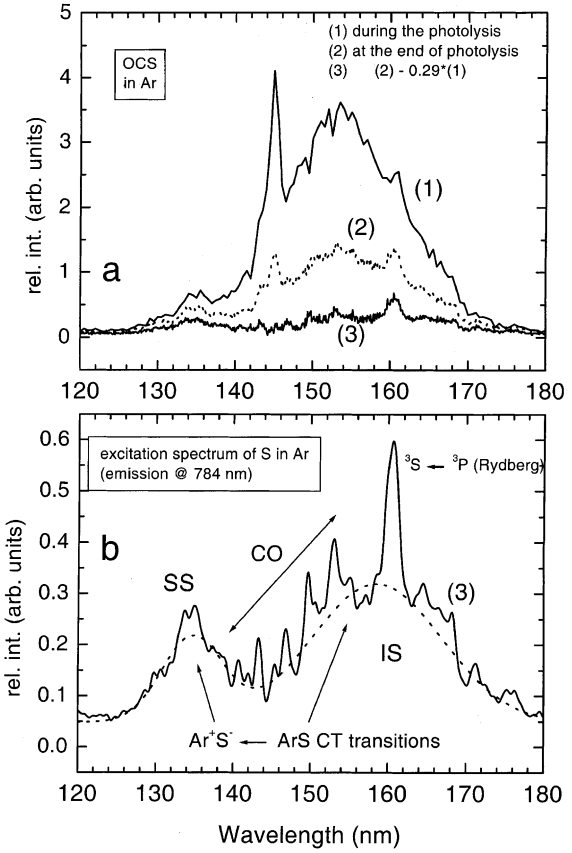

Fig. 3. (a) Excitation spectra during the photolysis, marked with (1); at the end of photolysis, marked with (2); and subtracted spectrum after scaling the intensity at 145 nm, marked with (3). Emission of S was monitored at 784 nm. (b) Subtracted spectrum from (a) marked with (3) fitted with two Gaussian curves (dotted lines). Absorption bands of ArS CT excitations in SS and IS as well as the S Rydberg transition are marked accordingly. Several bands between 138 and 158 nm are due to CO $A^1\Pi \leftarrow X^1\Sigma^+$ vibronic transitions.

of S the electron is promoted into the 4s orbital (configuration: $3s^23p^34s$), which is larger than the 3s orbital as in the case of O, that result in the ^3S state. Thus the electrostatic repulsion with the matrix surrounding is larger for S than for O Rydberg states. The present results are in full agreement with the results of Chergui et al. on NO in Ne matrices [13], where the matrix destabilization of 4s Rydberg states is larger than that of 3s Rydberg states compared to the corresponding energies in the gas-phase. The next feature of the

spectrum in Fig. 3b is the presence of two broad absorption bands, of which one centered around 135 nm and the other around 159 nm, the later being more intense and broader. These two bands resemble the CT absorption bands of O in Ar matrices centered around 132 and 145 nm (Fig. 4b), which we assigned to $Ar^+O^- \leftarrow ArO$ CT transitions in the substitutional site (SS) and interstitial site (IS), respectively [4]. Based on this similarity we assign the 135 and 159 nm bands in Fig. 3b to the $Ar^+S^- \leftarrow ArS$ CT transitions in the SS and IS, respectively. This assignment is further supported by the empirical calculations (vide infra). $^1S \rightarrow {}^1D$ emission of S in SS and IS of Ar and Kr lattices has been well studied by Zoval and Apkarian [18]. In the present study the detection of the CT transitions of S in Ar lattice in both these sites complements the studies of these authors. The fact that OCS could not be completely photolyzed with monochromatic synchrotron light and that the absorption spectra of S and OCS strongly overlap with each other, hindered us to undertake further detailed study on the site-selective spectroscopy of S in Ar matrices. The last feature of interest is the region between 140 and 160 nm, consisting several vibronic bands. Though relatively weak, these bands clearly correspond to the fourth positive system of CO ($A^1\Pi \leftarrow X^1\Sigma^+$ transition). It may be noted that these spectra were recorded by monitoring the $^1S \rightarrow {}^1D$ emission of S at 784 nm, which is shown in the insert of Fig. 1. Presence of the CO vibronic bands in the excitation spectrum shown in Fig. 3b may be due to photochemically induced energy transfer in S···CO van der Waals complexes, similar to the energy transfer in O···CO van der Waals complexes generated through VUV photolysis of CO_2 in Ar matrices [19].

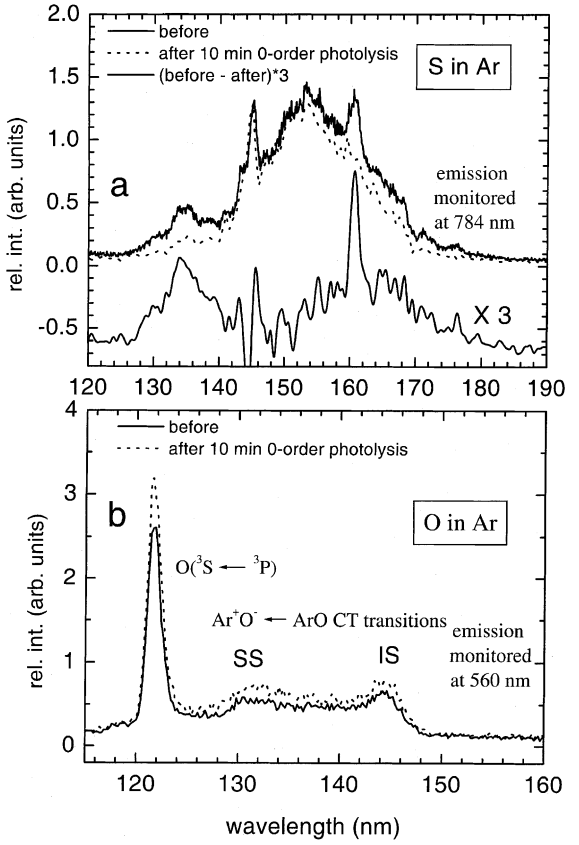

Fig. 4. (a) Excitation spectra at the end of photolysis of OCS with monochromatic synchrotron light, but before photolyzing with undispersed light (solid line), after 10 min photolysis with undispersed, zero-order synchrotron light (dotted line) and subtracted spectrum (before – after) photolysis with undispersed light. Emission was monitored at 784 nm. (b) Excitation spectra of O in Ar matrices before (solid line) and after (dotted line) photolysis with undispersed zero-order synchrotron light. $^1S \rightarrow {}^1D$ emission of O at 560 nm was monitored. The assignment of the bands is shown accordingly.

If we compare the excitation spectra shown in Fig. 3b with the absorption spectra in Fig. 2, it becomes immediately evident that the strong atomic absorption of S at 160.8 nm in the absorption spectra (Fig. 2b) appears as a relatively weak feature in the excitation spectra (Fig. 3b). On the other hand, the Ar^+S^- CT bands, which may be buried under the scattering continuum in the absorption spectra (Fig. 2a), are clearly seen in the excitation spectra (Fig. 3b). By noting that the excitation spectra were measured by monitoring the atomic transition $^1S \rightarrow {}^1D$ in S, we conclude that the molecular CT states undergo internal conversion more efficiently than the atomic Rydberg state $S(^3S)$ to populate the molecular $2^1\Sigma^+$ state corresponding to the atomic $S(^1S)$. The Rydberg state may directly undergo radiative relaxation to the ground-state $S(^3P)$ due to strongly allowed nature of this transition, bypassing the $S(^1S)$ state. However, the $(^3S \rightarrow {}^3P$ emission, which may occur in the VUV region around

160–180 nm, cannot be reached with the present detection system (detection limit >200 nm). We have attempted to measure the CT emission in the UV region between 200 and 400 nm, but without any success. Most likely the CT states undergo predominantly non-radiative relaxation to the $2^1\Sigma^+$ covalent state of ArS, corresponding to the ^{1}S state of S.

Photoinduced mobility of S atoms in rare-gas matrices has been well documented [1,20]. Due to the attractive or nearly non-repulsive nature of the ground-state Rg (^{1}S) and O [21] or S [22] in the ^{1}D state, mobility of O and S is proposed to occur in the ^{1}D state in Rg matrices [1]. However, it was a surprising observation for us that after near to 90% photolysis of the parent OCS molecules with monochromatic synchrotron radiation between 200 and 100 nm, when the matrices were irradiated with polychromatic (undispersed, zero-order grating position) light, the spectral features corresponding to S disappear to a great extent (Fig. 4a). The spectrum obtained after subtracting the excitation spectrum measured after photolysis with undispersed synchrotron light from the excitation spectrum measured at the end of photolysis with monochromatic synchrotron light, marked as (before – after) in Fig. 4a, is identical to the spectrum (3) shown in Fig. 3b. This clearly indicates photoinduced mobility of S atoms in Ar matrices caused by undispersed synchrotron radiation. The characteristic reflected wavelengths of the grating used at the 3m-NIM-1 monochromator spans the range between ~50 and 450 nm. On the other hand, the absorption spectra measured simultaneously during the measurement of the excitation spectra, shown in Fig. 2c, show only a small decrease in the 160.8 nm band of S. As we noted in the experimental section, the excitation spectra interrogate only the central part of the irradiated matrix receiving maximum photon flux, whereas the absorption spectra cover the whole irradiated region. Consequently, the S atoms must have moved away from the central region of the matrix and to a small extent they must have reacted with each other to form S_2, whose photolysis with the undispersed synchrotron light does not generate isolated S atoms back. Under similar conditions, irradiation of Ar matrices containing O (generated through photolysis of 0.1% O_2 in Ar) with polychromatic radiation rather increases the O atom population (Fig. 4b). This is a clear demonstration of more efficient photomobility of S atoms compared to O atoms in Ar matrices. If the photomobility of the S atoms should occur in the ^{1}D state [1], then the lifetime of the S(^{1}D) must be longer than that of O(^{1}D) in Ar matrices or that the collisional momentum transfer from the heavier S atoms to Ar should be more efficient than the lighter O atoms to Ar resulting in easier cage-exit of S atoms compared to O atoms. On the other hand, the photomobility by irradiating with VUV light, as in the present case, can also occur after the initial expansion and subsequent rearrangement of the first shell around the Rydberg S atoms.

3.2. Potential energy curves of the CT states

Successful prediction of the CT excitation energies of O in Ar and Kr matrices using empirical Rittner potentials, a combination of Coulomb attractive and Born–Mayer repulsive terms, and the stabilization due to the induced polarization of the matrix material [4], has encouraged us to use these empirical potential energy curves also to describe the Ar^+S^- CT states. In order to test the generality of this empirical deduction we have computed the potential energy curves for Rg^+O^- and Rg^+S^- (Rg = Ar, Kr and Xe) and then compared with available ab initio curves and experimental data. These results are discussed below:

$$E^R_{CT}(\text{gas}) = \left[E^{Rg}_{IP} - E^{X}_{EA} - \frac{e^2}{R}\right] + \left[A_{Rg^+X^-}\exp\left(-b_{Rg^+X^-}R\right)\right], \quad (1)$$

$$E^R_{CT}(\text{matrix}) = E^R_{CT}(\text{gas}) - \left(\frac{\varepsilon-1}{2\varepsilon+1}\right)\frac{e^2}{R}. \quad (2)$$

Potential energy curves of the CT states of Rg^+X^- (X = O or S) in the gas-phase using the Rittner potentials (Eq. (1)) are shown in Fig. 5a. Only the lower $j = 3/2$ state that results from spin–orbit coupling in Rg^+ is shown in each case. The upper $j = 1/2$ state runs parallel to the lower state with the corresponding difference of the spin–orbit splitting energy of the $Rg^+(^2P_j)$ states. Similarly, due to small spin–orbit splitting energy of $X^-(^2P_j)$,

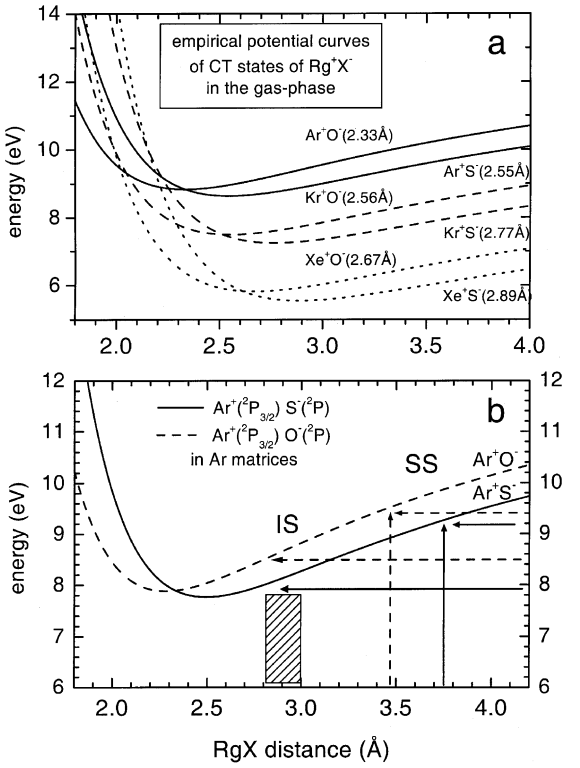

Fig. 5. (a) Empirical gas-phase potential energy curves of Rg^+X^- (Rg = Ar, Kr and Xe; X = O and S) derived using Eq. (1) and parameters given in Table 1. Solid line: Ar^+O^- and Ar^+S^-, dashed line: Kr^+O^- and Kr^+S^-, dotted line: Xe^+O^- and Xe^+S^-. An interatomic distance at the energy minimum of each curve is given in parentheses. (b) Empirical potential energy curves of Ar^+O^- and Ar^+S^- in Ar matrices derived using Eqs. (1) and (2) and parameters given in Table 1. Solid line: Ar^+S^- and dashed line: Ar^+O^-. Solid and dashed arrowhead lines pointing to each other locate vertical excitation energies in the SSs. Horizontal arrowhead lines point the regions of vertical excitations in the ISs.

spin–orbit coupling is neglected for the negative ions. It is important to note here that even after neglecting the spin–orbit coupling, 12 CT states of which six singlet and six triplet multiplicities with Σ, Π and Δ symmetries result from $Rg^+(^2P)X^-(^2P)$ configuration that results from the lowest ionized state of Rg. Thus, the empirical potential energy curve represents an average of these 12 states, which run close to each other at larger interionic separation but may diverge at shorter interionic separations due to correlation effect as well as mixing of ionic states with covalent states. For this reason and due to the fact that diatomic CT species may develop to polyatomic CT species when the same Rg acts as both the counter positive ion and the matrix material, we have purposefully omitted the CT emission of RgX in Rg matrices when comparing the empirically derived values with the experimental data. The parameters used to derive the empirical potential energy curves are collected in Table 1 and the present results are compared with experimental as well as ab initio results reported in the literature in Table 2. In the case of CT emission, the ground-state ($^3\Pi$) energies at the corresponding interatomic distances, taken from ab initio data (ArO and KrO [21]; XeO and XeS [8]; ArS [22]), were subtracted to derive the vertical transition energies. As can be seen in Table 2, the difference between the experimental band maxima and the empirically derived vertical energies of transitions involving the CT states of several RgX species is within a maximum of ±0.4 eV. Similarly, the agreement between the energy minima of the potential curves derived from ab initio and empirical methods is also very good, as shown in the last three rows of Table 2. Keeping in mind the simplicity of the empirical computations, the overall predictions of the vertical transition energies is excellent. After taking the stabilization due to induced polarization of the matrix medium (Eq. (2)), the empirical potential curves of the CT states of ArO and ArS are

Table 1
Parameters used in Eqs. (1) and (2) to derive empirical potential energy curves of the CT states of RgX (X = O,S)

Parameter	Ar	Kr	Xe	O	S
E_{IP}^{Rg}/E_{EA}^{X} (eV)	15.759	13.999	12.13	1.46	2.07
A_{Rg^+}/A_{X^-} (eV)	6411.8 (Cl)	18297 (Br)	33501 (I)	2619.4 (F)	6411.8 (Cl)
b_{Rg^+}/b_{X^-} (Å)	3.63681 (Cl)	3.54319 (Br)	3.51532 (I)	3.78383 (F)	3.63681 (Cl)
ε (dielectric constant of the matrix)	1.66	1.86			

The Born–Mayer interatomic potentials for the isoelectronic halogen atoms are taken from Abrahamson [26]. $e^2/R = 14.41$ eV.

Table 2
Empirically derived transition energies and minima of the potential energy curves of the CT states of RgX (X = O,S) compared with the experimental and ab initio results. For the last three rows E_{exp} should be read as $E_{ab\ inito}$

Species	Medium or method	Transition or location	E_{exp} (eV)	E_{calc} (eV)	ΔE (exp – calc)	Ref.
ArO	Gas-phase	CT $\rightarrow$ $^3\Pi$	8.27	8.54	−0.27	[27]
ArO	Ar matrix (SS)	CT $\leftarrow$ $^3\Pi$	9.4	9.5	−0.1	[4]
KrO	Gas-phase	CT $\rightarrow$ $^3\Pi$	6.89	7.27	−0.38	[27]
KrO	Kr matrix (SS)	CT $\leftarrow$ $^3\Pi$	7.75	7.79	−0.04	[4]
XeO	Gas-phase	CT $\rightarrow$ $^3\Pi$	5.3	5.53	−0.23	[27]
ArS	Ar matrix (SS)	CT $\leftarrow$ $^3\Pi$	9.18	9.32	−0.14	Present work
XeS	Gas-phase	CT $\rightarrow$ $^3\Pi$	5.46	5.13	0.33	[5]
KrS	Ab initio	CT minimum	~7.5 (3.1 Å)	7.25 (2.77 Å)	0.25	[7]
XeO	Ab initio	CT minimum	~6.1 (2.8 Å)	5.8 (2.67 Å)	0.3	[8]
XeS	Ab initio	CT minimum	~5.9 (3.3 Å)	5.55 (2.89 Å)	0.35	[8]

shown in Fig. 5b. In the SS with a nearest neighbour distance of 3.75 Å in an unperturbed lattice, ArO exists as a van der Waals molecule in the $^3\Pi$ ground-state at an interatomic separation of 3.47 Å [23], whereas due to the van der Waals minimum of the $^3\Pi$ ground-state of ArS at 3.79 Å [24], the S atoms occupy perfectly the substitutional cavity. The vertical transition energies of ArO (at 3.47 Å) and ArS (at 3.79 Å) in the SS, as shown in Fig. 5, differ minimally by ca. 0.2 eV, which is in excellent agreement with the experimental observation: band maxima of the CT transitions in ArO (132 nm) and ArS (135 nm) in Ar matrices. On the other hand, in the IS, with the cavity radius of 2.65 Å in an unperturbed Ar lattice, both O as well as S cannot be accommodated without distorting the surrounding. Thus, in the case of O in Ar, we have shown that by taking the 0.38 Å expansion of the axial Ar atoms in the first shell of the IS [25], the empirical vertical excitation energy of ArO at 2.83 Å reproduces the experimental data well. In the case of S in IS of Ar stronger distortion of the cavity is to be expected due to larger van der Waals radius of S. Accordingly, the restructuring of the IS site should occur more often with S than O, especially in defect surroundings. Thus, we expect a wide distribution of ArS distances in the IS, as marked in Fig. 5b, which is also reflected in the much broader absorptions band at 159 nm compared to the one at 135 nm. Further, the CT excitation may involve delocalization of the positive charge (hole) on all the six surrounding Ar atoms, something like formation of an excited supermolecule, or that the hole is localized on only one Ar atom [4]. Irrespective of the nature of the upper CT state, we expect destabilization of the ground-state of Ar_nS ($n = 1$–6) in the IS due to the repulsive nature of the ArS $^3\Pi$ ground-state at shorter Ar$\cdots$S interatomic distances [22], which should be taken into account to compute the CT vertical excitation energies. Considering all these factors and noting that the ground-state ($^3\Pi$) energy of ArS is 0.14 eV at 2.9 Å [22], the predicted vertical CT transition wavelength of 155 nm in the IS is in good agreement with the experimental value of 159 nm.

4. Conclusions

CT transitions of ArS in the substitutional and interstitial sites and Rydberg excitation of S have been observed for the first time from matrix isolated S atoms that have been generated through VUV photolysis of OCS in Ar matrices. Empirically predicted excitation energies of the transitions from the repulsive ground-state to the CT states are in good agreement with the experimental data. S atoms are found to be more photomobile than O atoms in Ar matrices.

Acknowledgements

A part of the present work is financed by DFG (Grant No. GU 413/3). Travel support by DESY through BESSY is also acknowledged gratefully.

References

[1] V.A. Apkarian, N. Schwentner, Chem. Rev. 99 (1999) 1481.
[2] L. Khriachtchev, M. Pettersson, N. Runeberg, J. Lundell, M. Räsänen, Nature (London) 406 (2000) 874.
[3] N. Runeberg, M. Pettersson, L. Khriachtchev, J. Lundell, M. Räsänen, J. Chem. Phys. 114 (2001) 836.
[4] M.S. Gudipati, M. Kalb, Chem. Phys. Lett. 307 (1999) 27.
[5] J. Xu, D.W. Setser, J.K. Ku, Chem. Phys. Lett. 132 (1986) 427.
[6] S. Tanaka, H. Kajihara, S. Koda, V.A. Apkarian, Chem. Phys. Lett. 233 (1995) 555.
[7] A.V. Nemukhin, B.L. Grigorenko, A.A. Granovsky, Chem. Phys. Lett. 301 (1999) 287.
[8] M. Yamanishi, K. Hirao, K. Yamashita, J. Chem. Phys. 108 (1998) 1514.
[9] A. Klein, M. Kalb, M.S. Gudipati, J. Phys. Chem. A 103 (1999) 3843.
[10] A. Hishikawa, K. Ohde, R. Itakura, S. Liu, K. Yamanouchi, K. Yamashita, J. Phys. Chem. 101 (1997) 694.
[11] R.V. Taylor, W.C. Walker, K.M. Monahan, V. Rehn, J. Chem. Phys. 72 (1980) 6743.
[12] R. Feng, G. Cooper, C.E. Brion, Chem. Phys. 252 (2000) 359.
[13] M. Chergui, N. Schwentner, W. Böhmer, J. Chem. Phys. 85 (1986) 2472.
[14] S.S. Tayal, Astrophys. J. 497 (1998) 493.
[15] W.F. Chan, G. Cooper, C.E. Brion, Chem. Phys. 170 (1993) 123.
[16] M.S. Gudipati, Chem. Phys. Lett. 248 (1996) 452.
[17] E. Biémont, H.P. Garnir, S.R. Federman, Z.S. Li, S. Svanberg, Astrophys. J. 502 (1998) 1010.
[18] J. Zoval, V.A. Apkarian, J. Phys. Chem. 98 (1994) 7945.
[19] R. Wagner, F. Schouren, M.S. Gudipati, J. Phys. Chem. A 104 (2000) 3593.
[20] L. Khriachtchev, M. Pettersson, S. Pehkonen, E. Isoniemi, M. Räsänen, J. Chem. Phys. 111 (1999) 1650.
[21] T.H. Dunning Jr., P.J. Hay, J. Chem. Phys. 66 (1977) 3767.
[22] T. Kiljunen, J. Eloranta, H. Kunttu, L. Khriachtchev, M. Pettersson, M. Räsänen, J. Chem. Phys. 112 (2000) 7475.
[23] V. Aquilanti, R. Candori, F. Pirani, J. Chem. Phys. 89 (1988) 6157.
[24] V. Aquilanti, D. Ascenzi, E. Braca, D. Cappelletti, F. Pirani, Phys. Chem. Chem. Phys. 2 (2000) 4081.
[25] D. Maillard, J. Fournier, H.H. Mohammed, C. Girardet, J. Chem. Phys. 78 (1983) 5480.
[26] A.A. Abrahamson, Phys. Rev. 178 (1969) 76.
[27] S. Neeser, M. Voitik, H. Langhoff, J. Chem. Phys. 102 (1995) 1639.